Biometrics 00, 1–??
?? 2019
DOI: 10.1111/j.1541-0420.2005.00454.x

A latent capture history model for digital aerial surveys

D. L. Borchers[1,*], P. Nightingale[2], B. C. Stevenson[3], and R. M. Fewster[3]

[1]University of St Andrews, Centre for Research into Ecological and Environmental Modelling, St Andrews, Fife, UK

[2]Department of Computer Science, University of York, Deramore Lane, Heslington, York, UK

[3]Department of Statistics, University of Auckland, Private Bag 92019, Auckland, New Zealand

email: dlb@st-andrews.ac.uk

Summary: We anticipate that unmanned aerial vehicles will become popular wildlife survey platforms. Because detecting animals from the air is imperfect, we develop a mark-recapture line-transect method using two digital cameras, possibly mounted on one aircraft, which cover the same area with a short time delay between them. Animal movement between the passage of the cameras introduces uncertainty in individual identity, so individual capture histories are unobservable and are treated as latent variables. We obtain the likelihood for mark-recapture line transects without capture histories by automatically enumerating all possibilities within segments of the transect that contain ambiguous identities, instead of attempting to decide identities in a prior step. We call this method 'Latent Capture-history Enumeration' (LCE). We include an availability model for species that are periodically unavailable for detection, such as cetaceans that are undetectable while diving. External data are needed to estimate the availability cycle length, but not the mean availability rate, if the full availability model is employed.

We compare the LCE method with the recently-developed cluster capture-recapture method (CCR), which uses a Palm likelihood approximation, providing the first comparison of CCR with maximum likelihood. The LCE estimator has slightly lower variance, more so as sample size increases, and close to nominal covarage probabilities. Both methods are approximately unbiased. We illustrate with semi-synthetic data from a harbor porpoise survey.

Key words: Availability bias; Double-observer survey; Line transect; Mark-recapture; Movement model; Poisson process.

This paper has been submitted for consideration for publication in *Biometrics*

1. Introduction

Aerial surveys of wildlife populations allow large areas of land or sea to be surveyed at relatively low expense (Henkel et al., 2007; Hammond et al., 2017). We anticipate that aerial surveys with human observers will increasingly be replaced by unmanned aerial vehicle (UAV) surveys using digital video or still cameras. In this paper we develop a method of estimating animal density from cameras deployed from UAVs.

Human observers can search as much as 1000m either side of an aircraft. Detections of animals decrease with distance from the aircraft, an effect that is modeled using a detection function. By contrast, aerial footage from UAV-mounted cameras has a much narrower field of view — perhaps 100m to either side — and detectability can often be assumed to be constant within this zone, so that a distance-dependent detection function is not needed.

Conventional line transect analyses assume that animals are detected with certainty if they are at distance zero from the transect line, which in our case is the projection of the aircraft's path on the ground. If this assumption cannot be met, extensions based on mark-recapture methods are employed: see Burt et al. (2014) for an overview. The basis of these extensions is to have two observers who search the area independently of each other. They serve as two 'capture occasions', and animals detected by both observers are described as recaptures or duplicates. The mark-recapture design enables us to estimate the detection probability of each observer, conditional on detection by the other observer, and therefore to adjust for imperfect detection at distance zero. In the case of narrow-strip aerial surveys from UAVs, imperfect detection can result from animals being indistinct or obscured in digital images, so a mark-recapture design may be necessary even if detectability is constant with respect to distance.

Animals of some species may spend a proportion of their time entirely unavailable for detection. For example, whales are unavailable while diving, and seals are unavailable at haul-out

sites while they are at sea. In the case of acoustic surveys of calling animals, animals are only available when vocalising. If some animals are systematically unavailable to both observers, then the unavailable portion of the population is unsampled, so there is no information from which to estimate how large this portion is. An ideal sampling design ensures that all animals are subject to the same detection model, so that the sample is representative of the entire population. In the case of animals that are periodically unavailable, for example due to diving, this can be accomplished by incorporating an availability model into the analysis and sampling at more than one time.

One way of sampling twice is to have two aircraft follow the same transect at a fixed time delay. Ensuring that the narrow search strips of two UAVs overlap adequately can be difficult in some environments and a cheaper alternative is to mount two cameras on a single aircraft: one forward-pointing, the other rear-pointing. These can be engineered so that the rear-pointing camera records the same area as the forward-pointing camera after a time delay of several seconds. This separation generates data with which we can model the availability cycle, as long as there is a chance that the availability status of an animal changes between the passage of the two cameras. For example, a whale might dive or surface during this time interval. In practice, the time delay will need to be sufficiently long relative to the duration of the diving cycle to ensure that the data are adequate to fit the availability model.

Mounting both cameras on the same UAV has the advantage of creating a different viewing aspect for the two cameras: an animal that is obscured from one camera by a bush or shadow might be detectable from the other camera. Likewise, the longer time separation generated by running two UAVs in succession creates the opportunity for either camera to detect an animal that was undetected by the other, due to changes in the animal's position, sunlight, or wind. The two-camera design therefore offers general potential for conducting mark-recapture line transect surveys from the air, regardless of whether or not an availability cycle is involved.

There are two complications. Firstly, because animals may move between the passage of the two cameras, there is uncertainty in whether detections in similar locations by the two cameras are the same animal or two different animals. We describe this as *uncertainty in capture history*. Each detected animal has a true capture history specifying which of the two cameras detected it, with capture histories $(1, 0)$, $(0, 1)$, and $(1, 1)$ corresponding respectively to detection by only the first camera, only the second camera, or both cameras. When animals are detected from the air, there are usually inadequate visible features for distinguishing between individuals, so recaptures are determined purely on the basis of spatial location and detection time. The longer the time elapsed between the passage of the two cameras, the more difficult it is to distinguish between recaptures of a single individual, and captures of two different individuals. Rather than the capture histories being observed data, as they are in conventional capture-recapture studies, they are now latent variables.

Secondly, although separation in time allows us to deal with availability processes such as diving, there is likely to be dependence between the animal's availability state at the passage of the two cameras, so we are forced to adopt a model that accommodates this dependence. The dependence is reduced as the time delay between the passage of the cameras increases. However, we demonstrate below that the dependence never reduces to zero if animals are mobile, because animal movement in and out of the field of view of the cameras is itself an availability process. Moreover, while longer delays may reduce the dependence between cameras, they exacerbate the problem of capture-history uncertainty.

We develop an analysis framework suitable for two-camera aerial surveys. We explicitly model animal movement into and out of the detection strip between the passage of the two cameras, corresponding to an 'in/out' availability process that induces dependence between the two cameras. For diving animals, we further consider an 'up/down' availability process by modeling the diving cycle. As noted by Stevenson et al. (2019), two-observer survey data

do not contain sufficient information to identify all parameters of the diving model, if the time delay between cameras is less than the mean dive-cycle duration. In that case, one parameter must be estimated from external data: we take this to be the mean dive-cycle duration itself. We derive our methods in generality including both in/out and up/down availability processes, but the methodology is equally applicable when only the in/out process is required, and in that case there is no need for external data.

To fit the two-camera model we use a full maximum-likelihood approach. We assemble the likelihood by identifying segments of the transect line that have ambiguous animal identities, and enumerating all possible matchings within each segment. For reasonably low density, enumeration is manageable within each segment, and our approach is computationally feasible using a constraint programming algorithm. Conditional on a set of matchings, we use a hidden Markov model formulation of the likelihood, with states reflecting animals' availability to be detected. This creates a general and extendable framework for two-camera scenarios. We call our new approach the latent capture-history enumeration (LCE) method.

Previous literature has devoted substantial attention to each of the problems of availability and uncertain capture histories, but rarely together. Availability models for double-observer line transect surveys were developed by Borchers et al. (2013), Langrock et al. (2013), and Borchers and Langrock (2015). Most previous work on uncertain capture histories has focused on methods for resolving uncertainties before fitting conventional models. Pike and Doniol-Valcroze (2015) used a logistic regression technique to decide on an optimal dissimilarity score between pairs of detections, then established a threshold score within which pairs would be resolved as duplicates. Hamilton et al. (2018) devised estimates of the duplicate probability for each pair of detections, and repeatedly resampled from these probabilities within a bootstrap scheme to create a new resolved dataset at each iteration. Other work on latent capture histories has treated the case where observed histories are predictable, but

non-invertible, transformations of the latent histories (e.g. Zhang et al., 2019; Bonner and Holmberg, 2013; Link et al., 2010). This contrasts with our case where no capture histories are observed: only a stream of detections from each camera in continuous time and space.

Our approach is most similar to that of Hiby and Lovell (1998) and Stevenson et al. (2019). Hiby and Lovell (1998) included both an availability model and uncertain capture histories in their analysis, and they maximized a log-likelihood obtained by summing over possible pairs of detections. They did not allow animal movement in the direction of aircraft travel, and some aspects of their implementation were not explicit. Neglecting animal movement in the direction of aircraft travel is not a problem for observers that travel much faster than the animals, but it is a problem for slow-moving observers. Stevenson et al. (2019) derived an alternative approach using the new technique of cluster capture-recapture (CCR; see Fewster et al., 2016). In CCR, the locations of detections are treated as a clustered point-process and the model is fitted using an approximation to the Palm likelihood (Tanaka et al., 2008), which is a likelihood of pairwise distances over all pairs of detections.

The CCR method is asymptotically consistent and remains computationally efficient at high animal densities, unlike the LCE method we present here. However, due to the approximation step it is not a maximum likelihood method, and its performance has never been compared against that of maximum likelihood due to the difficulty of computing likelihoods in the scenarios for which CCR is intended. Another key output of the present work is therefore the first comparison between CCR and maximum likelihood.

2. Models for movement and availability

Two observers move along a transect line, one behind the other, searching a strip of half-width w. They move at constant speed v and are separated by a time-lag l and distance vl. We use the general term 'observers' and develop the model for lags l of any size, but we anticipate that the two observers are most likely to be two cameras on the same UAV

(Figure 1).

We use two coordinates for location: the forward coordinate along the transect line, and the transverse coordinate perpendicular to the line. We say that an observer 'passes over' an animal at the instant that their forward coordinates coincide, regardless of the animal's transverse coordinate at that instant. We assume that observer speed exceeds animal speed, so the time at which each observer passes over each animal is well-defined.

Animals may move between the passage of the two observers. We model this as a Brownian motion, such that the animal's displacement over time t follows a bivariate normal distribution with mean $(0, 0)$ and variance $\boldsymbol{\Sigma}(t) = \sigma^2 t \boldsymbol{I}$, where $\boldsymbol{I}$ is the 2×2 identity matrix.

[Figure 1 about here.]

2.1 *Forward movement*

For a given animal, the time elapsed between the passage of the first and second observers overhead is a random variable T. We show in Web Appendix A that T has probability density function (PDF)

$$f_T(t) = \frac{vl \exp\left\{-\frac{v^2(l-t)^2}{2\sigma^2 t}\right\}}{\sqrt{2\pi\sigma^2 t^3}} \text{ for } t > 0, \text{ and } f_T(t) = 0 \text{ otherwise.} \quad (1)$$

2.2 *Transverse movement and in/out availability*

The survey design involves two observers detecting animals within a strip of width w either side of the line. As animals may move into or out of the detection zone between the passage of the two observers, we consider the survey area to constitute a wider strip of width $b > w$ either side of the line, where the buffer b is chosen such that there is negligibly small probability that animals beyond b at the passage of the first observer will be within the searched strip w at the passage of the second. The buffered strip of width $2b$ therefore covers all animals that may be exposed to detection.

Let Y_0 be the signed distance of an animal to the right of the transect line when the first

observer passes overhead, and Y_t be this distance time t later. We assume that $Y_0 \sim U(-b, b)$, independently for all animals. Our movement model implies that $Y_t - Y_0 \sim N(0, \sigma^2 t)$.

For any animal within the buffered strip $2b$ at the passage of the first observer, let the binary random variable Z_t be 1 if the animal is within the detection zone of width $2w$ at time t, and 0 otherwise. Thus Z_t describes the animal's in/out availability for detection at time t. The probability $\mathbb{P}(Z_t = 0 \mid Z_0 = 1)$ that an animal moves from inside the detection zone at time $t = 0$ to outside it at time $t > 0$, and the probability $\mathbb{P}(Z_t = 1 \mid Z_0 = 0)$ that it moves from outside to inside the detection zone, are

$$p_{IO}(t) = \mathbb{P}(Z_t = 0 \mid Z_0 = 1) = \frac{1}{w} \int_0^w \left\{ \Phi(y - w; \sigma^2 t) + \Phi(-y - w; \sigma^2 t) \right\} dy \quad (2)$$

$$p_{OI}(t) = \mathbb{P}(Z_t = 1 \mid Z_0 = 0) = \frac{1}{b - w} \int_w^b \left\{ \Phi(y + w; \sigma^2 t) - \Phi(y - w; \sigma^2 t) \right\} dy \quad (3)$$

where $\Phi(\cdot; \sigma^2 t)$ is the cumulative distribution function of a normal random variable with mean zero and variance $\sigma^2 t$.

We model in/out availability as a two-state Markov process with transition probabilities over an interval of time t given by Eqns (2) and (3):

$$\boldsymbol{M}(t) = \begin{pmatrix} 1 - p_{IO}(t) & p_{IO}(t) \\ p_{OI}(t) & 1 - p_{OI}(t) \end{pmatrix}, \quad (4)$$

with stationary distribution $(w/b,\ 1 - w/b)$.

2.3 *Diving behavior and up/down availability*

We define a random variable U_t to be 1 if an animal is in the near-surface state and so available for detection at time t, and to be 0 otherwise. We further define $(U_t)_{t \geqslant 0}$ to be a two-state continuous-time Markov chain such that the time spent in state 1 (the near-surface state) is an exponential random variable with expected value κ, and the time spent in state 2 (the diving state) is an exponential random variable with expected value $\tau - \kappa$, where τ is the expected dive cycle duration. The up/down state transition probability matrix at time

separation t is $\boldsymbol{U}(t) = \exp(\boldsymbol{Q}t)$, where $\exp(\ )$ is the matrix exponential function and the Markov transition rate matrix $\boldsymbol{Q}$ is

$$\boldsymbol{Q} = \begin{pmatrix} -\frac{1}{\kappa} & \frac{1}{\kappa} \\ \frac{1}{\tau-\kappa} & -\frac{1}{\tau-\kappa} \end{pmatrix}. \tag{5}$$

The stationary distribution of the Markov chain is $(\gamma,\ 1-\gamma)$, where $\gamma = \kappa/\tau$.

2.4 *Combined availability model*

The possibilities of being in or out of the detection zone, and up or down with respect to diving, generate four states that animals can occupy. These are, up and in: $U_t = 1$, $Z_t = 1$; up and out: $U_t = 1$, $Z_t = 0$; down and in: $U_t = 0$, $Z_t = 1$; and down and out: $U_t = 0$, $Z_t = 0$. We number the states 1 to 4 in that order. We assume that the up/down state is independent of the in/out state, which is equivalent to an assumption that animals are not disturbed by the aircraft. The matrix of transition probabilities between these states at time separation t is then the Kronecker product $\boldsymbol{\Gamma}(t) = \boldsymbol{U}(t) \otimes \boldsymbol{M}(t)$. Using a matrix formulation for $\boldsymbol{\Gamma}(t)$ provides an extendable and computationally efficient way of dealing with the hidden states 2, 3, and 4. The stationary distribution for the four-state Markov process is

$$\boldsymbol{\delta} = \left(\gamma\frac{w}{b},\ \gamma\left(1-\frac{w}{b}\right),\ (1-\gamma)\frac{w}{b},\ (1-\gamma)\left(1-\frac{w}{b}\right)\right). \tag{6}$$

3. Detection model

We assume that the probability that an animal is in each state at the time the first observer passes over it is given by the stationary distribution $\boldsymbol{\delta}$, and hence that its state distribution after a waiting time t, when the second observer passes it, is $\boldsymbol{\delta\Gamma}(t)$.

Define the binary variable X_{ij} to be 1 if animal i is detected by observer j and zero otherwise. We model X_{ij} as a state-dependent Bernoulli random variable with parameter $p_j(c) = \Pr(X_{ij} = 1 \mid C_{ij} = c)$ where C_{ij} is the state of animal i when observer j passes over it, and $c \in \{1, 2, 3, 4\}$. It follows that X_{ij} $(j \in \{1, 2\})$ are observations from a Markov

modulated Bernoulli process.

It is convenient to arrange the state-dependent probability mass functions of X_{ij} in a diagonal matrix (see Zucchini et al., 2016, Eqn 2.13). For observer j, this matrix is

$$\boldsymbol{P_j}(x_{ij}) = \begin{array}{c} \begin{array}{cccc} \text{up,in} & \text{up,out} & \text{down,in} & \text{down,out} \end{array} \\ \begin{pmatrix} \text{Bern}(x_{ij}; p_j(1)) & 0 & 0 & 0 \\ 0 & 1 - x_{ij} & 0 & 0 \\ 0 & 0 & \text{Bern}(x_{ij}; p_j(3)) & 0 \\ 0 & 0 & 0 & 1 - x_{ij} \end{pmatrix} \end{array} \tag{7}$$

where $\text{Bern}\big(x_{ij}; p_j(c)\big) \equiv p_j(c)^{x_{ij}}\{1 - p_j(c)\}^{1-x_{ij}}$. This allows detection of animals when 'down', but not when 'out'. We now assume that $p_j(3) = 0$, so that only animals in the 'up' and 'in' state can be detected, but in general this need not be the case.

Let t_i be the time elapsed between the passage of the first and second observers over animal i. Conditional on t_i, the probability of observing capture history (x_{i1}, x_{i2}) for animal i can be expressed as the following matrix product, which efficiently sums over hidden states:

$$\mathbb{P}(x_{i1}, x_{i2} \mid t_i) \;=\; \boldsymbol{\delta P_1}(x_{i1})\boldsymbol{\Gamma}(t_i)\boldsymbol{P_2}(x_{i2})\mathbf{1}\,, \tag{8}$$

where $\mathbf{1}$ is a column vector of ones. We label the three observable capture histories as $\tilde{\omega}_1 = (0, 1)$, $\tilde{\omega}_2 = (1, 0)$, and $\tilde{\omega}_3 = (1, 1)$, and define $q_k(t) = \mathbb{P}(\,\tilde{\omega}_k \mid t)$ as given in (8). The overall probability of capture history $\tilde{\omega}_k$ is then

$$\tilde{q}_k = \mathbb{P}(\,\tilde{\omega}_k\,) = E_t\left\{\mathbb{P}(\,\tilde{\omega}_k \mid t)\right\} = \int q_k(t) f_T(t)\, dt\,. \tag{9}$$

4. Survey model

We assume that the number and locations of animals in the forward direction, within distance b of the transect line at the time that the first observer passes overhead, are governed by a Poisson process with intensity $D(s)$ at along-transect location s. We derive the likelihood by supposing that the capture history ω_i of each animal i is known. We will later revoke this

requirement by marginalizing over all possible assignments of detections to capture histories.

Let $\boldsymbol{s} = (s_1, \ldots, s_n)$ be the observed forward locations of the n detected animals at the time of first detection. We can write $\boldsymbol{s} = \left(\boldsymbol{s}^{(1)}, \boldsymbol{s}^{(2)}, \boldsymbol{s}^{(3)}\right)$, where $\boldsymbol{s}^{(k)}$ corresponds to locations of animals with capture history $\tilde{\omega}_k$ for $k = 1, 2, 3$. Each set of locations $\boldsymbol{s}^{(k)}$ arises from thinning the overall Poisson process by probability $\tilde{q}_k$. Because multinomial splitting of a Poisson process produces independent Poisson subprocesses, the likelihood of $\boldsymbol{s}$ is the product of the three likelihoods from the thinned subprocesses. For animals with capture history $\tilde{\omega}_3 = (1, 1)$, we observe the time delay t between detection by the first and second observers, in addition to the locations of the animals at these times. The time that it takes animals to move between the two locations at which they were observed provides information about the movement parameter σ. The PDF of waiting time T, conditional on the capture history being $\tilde{\omega}_3$, is

$$f_{T|\,\omega}(t \mid \tilde{\omega}_3) = \frac{f_T(t)\,\mathbb{P}(\tilde{\omega}_3 \mid t)}{\mathbb{P}(\tilde{\omega}_3)} = \frac{f_T(t)\,q_3(t)}{\tilde{q}_3}\,, \tag{10}$$

where the right-hand side of (10) is obtained from Equations (1), (8), and (9). This PDF is included as an auxiliary component to the Poisson process likelihood for $\boldsymbol{s}^{(3)}$.

Let L be the total transect length of the survey, and let n_k be the number of observations of capture history $k = 1, 2, 3$, with $n_1 + n_2 + n_3 = n$. Let $\tilde{q}_\cdot = \tilde{q}_1 + \tilde{q}_2 + \tilde{q}_3$ be the overall probability of detection. We write $\boldsymbol{s}$, $\boldsymbol{\omega}$, and $\boldsymbol{t}$ for the locations, capture histories, and (where available) time delays for animals $i = 1, \ldots, n$. The parameter vector is $\boldsymbol{\theta}$ (see Section 4.1). The likelihood is:

$$\mathcal{L}(\boldsymbol{\theta}\,;\,\boldsymbol{s}, \boldsymbol{\omega}, \boldsymbol{t}) = \frac{\exp\left\{-\int_0^L D(u)\tilde{q}_\cdot\,du\right\}}{n_1!\,n_2!\,n_3!} \left\{\prod_{i=1}^{n} D(s_i)\right\} \tilde{q}_1^{n_1}\,\tilde{q}_2^{n_2} \prod_{i\,:\,\omega_i = \tilde{\omega}_3} \left\{f_T(t_i)\,q_3(t_i)\right\}. \tag{11}$$

4.1 *Model parameters*

The model has four kinds of parameters:

Density parameters: In the case of the homogenous Poisson process there is one parameter, η, such that $D = e^{\eta}$. When density varies with covariates, η is replaced by a linear

predictor involving a parameter vector.

Dive cycle parameters: The two-state dive cycle model described above is parametrized in terms of the mean dive cycle length, τ, and the mean proportion of time in the near-surface state, γ, which are linked to parameters α_τ and α_γ via log and logit links: $\tau = e^{\alpha_\tau}$ and $\gamma = e^{\alpha_\gamma}/(1 + e^{\alpha_\gamma})$.

Movement parameters: The animal movement model has one parameter, σ, which we model using a log link: $\sigma = e^{\phi}$.

Detection parameters: Assuming that animals are only detectable when in state $c = 1$ (up, in), we have two Bernoulli parameters to model: $p_1(1)$ and $p_2(1)$. These can be modeled using logit link functions. If the observers are identical digital detectors, it may be reasonable to assume these two probabilities are identical, i.e. $p_1(1) = p_2(1) = p = e^{\beta}/(1 + e^{\beta})$.

Covariates can be incorporated by replacing the corresponding scalar parameter on the link scale with a suitable linear predictor involving the covariates.

We focus below on the constant density model with identical detectors and no covariates, which has five parameters: $\boldsymbol{\theta} = (\eta, \alpha_\gamma, \alpha_\tau, \phi, \beta)$. Stevenson et al. (2019) showed that these are not all identifiable from the two-observer survey design. For the detection model, they assumed that $p = e^{\beta}/(1 + e^{\beta}) = 1$. This is reasonable for digital aerial surveys conducted in calm sea states, if we define the near-surface state to be 'at or breaking the surface': a state that is easily observed. The field of view of a digital camera is such that objects towards the periphery of the image are typically as easily detected as objects in the centre of the image, so a detection function that drops off with distance from the line is not needed.

Stevenson et al. (2019) also showed that even when p is known, only two of $(\eta, \alpha_\gamma, \alpha_\tau)$ are identifiable, so one of these parameters must be estimated using external data. We follow Stevenson et al. (2019) and Hiby and Lovell (1998) and assume that the mean dive cycle duration $\tau = e^{\alpha_\tau}$ is estimated separately, so we treat it as known in the present survey. In

what follows, we therefore assume that detection of animals in the up/in state is certain ($p = 1$); we use external estimates to set τ; and we estimate the remaining three parameters. These constitute the density, D; the mean proportion of time in the near-surface state, γ; and the movement parameter, σ. The parameter vector is therefore $\boldsymbol{\theta} = (\eta, \alpha_\gamma, \phi)$.

5. Marginalising over the latent capture histories

The likelihood (11) is formulated under the supposition that the capture history vector $\boldsymbol{\omega}$ is known for animals $i = 1, \ldots, n$. However, the core problem when observers are separated in time is that the capture histories cannot be known with certainty: they are latent variables. Here we address this problem by enumerating all plausible combinations of latent capture histories. We marginalize the likelihood by summing over the individual likelihoods for every plausible capture history combination. We refer to each combination of capture histories as a 'pairing', since once the pairs of detections with capture history $\tilde{\omega}_3 = (1, 1)$ have been decided, the capture histories $(0, 1)$ or $(1, 0)$ of all other detections are determined, because we know which of the two observers made each detection.

Calling the mth set of pairings $\boldsymbol{\omega}^{(m)}$, and the associated vectors of first-detection locations and time delays $\boldsymbol{s}^{(m)}$ and $\boldsymbol{t}^{(m)}$ respectively, we obtain the likelihood for the parameters $\boldsymbol{\theta}$ as

$$\mathcal{L}(\boldsymbol{\theta}) \;=\; \sum_{m=1}^{M} \mathcal{L}\left(\boldsymbol{\theta}; \boldsymbol{s}^{(m)}, \boldsymbol{\omega}^{(m)}, \boldsymbol{t}^{(m)}\right) , \tag{12}$$

where M is the number of plausible pairings.

While this likelihood is easy to write down, it is challenging to evaluate because we need to enumerate all M plausible combinations $\boldsymbol{\omega}^{(m)}$. For any but very small sample sizes, the number M of possible pairings is very large. We tackle this problem by first partitioning the location vector $\boldsymbol{s}$ into subsets between which paired detections are impossible, to reduce the number of plausible pairings, and then using a constraint programming technique for efficient enumeration of all possible pairings within subsets. The constraint programming

algorithm is described in Web Appendix B.

5.1 *Subdivision of* $\boldsymbol{s}$

We partition $\boldsymbol{s}$ by 'cutting' the transect line between adjacent detections (by either observer) that are separated by a distance greater than a maximum possible distance that an animal could have moved between the two observers passing over it (d_{max}). This distance d_{max} must be decided using knowledge of the movement speed and behavior of the target species. A suitable value for d_{max} can be chosen by doing inference at a range of plausible values to find where estimates become insensitive to d_{max}. The cost of setting d_{max} too large is in computational speed; the cost of setting d_{max} too small is positive bias in estimation of D, since setting d_{max} too small will result in some animals with true capture history $(1, 1)$ being assigned capture history $(0, 1)$ or $(1, 0)$.

Having divided the transect line into R segments, we enumerate the possible pairings $\boldsymbol{\omega}^{(m_r)}$ for segments $r = 1, \ldots, R$ and obtain the likelihood as

$$\mathcal{L}(\boldsymbol{\theta}) \;=\; \prod_{r=1}^{R} \sum_{m_r=1}^{M_r} \mathcal{L}\left(\boldsymbol{\theta}; \boldsymbol{s}^{(m_r)}, \boldsymbol{\omega}^{(m_r)}, \boldsymbol{t}^{(m_r)}\right) , \tag{13}$$

where M_r is the number of possible pairings in segment r. When d_{max} is substantially smaller than most of the distances between detections by different observers, segmentation can lead to a massive reduction in computation time.

5.2 *Interval estimation*

We estimate the variances of parameters using the inverse of the Hessian obtained in the fitting process. Confidence intervals for the parameters D, σ and γ are gained from the inverse log transformation of confidence intervals for η and ϕ, and the inverse logit transformation of α_γ, assuming normality of the maximum likelihood estimators of these parameters.

6. Application

We use the term 'Latent Capture-history Enumeration' method, or LCE, to describe our framework. We developed this method in anticipation of digital aerial survey data becoming widely used, but, pending the availability of analysis methods such as the LCE method developed here, such data are not yet available. We therefore estimate density from the semi-synthetic data used by Stevenson et al. (2019). These data are taken from an aerial survey of harbor porpoise (*Phocoena phocoena*) in the North Sea using human observers, compiled from periods when the aircraft circled back over its transect after a lag of $l = 248$ seconds. The two observers correspond to the two passes of the aircraft. Only data in a narrow strip of half-width $w = 0.125$ km are included, to mimic the narrow field of view and perfect near-surface detection characteristic of digital observers. The data for both the LCE and CCR methods comprise the two sets of locations of detected animals: $\boldsymbol{s}_1$ for those detected by observer 1, and $\boldsymbol{s}_2$ for those detected by observer 2. Which of the observer 1 detections are recaptured by observer 2 is unknown, and the LCE method considers all possibilities.

A lag of $l = 248$ seconds is longer than plausible values for τ (Stevenson et al., 2019), and so the surfacing states of an animal at the times the observers pass are independent and the estimator is robust to unknown τ. For shorter lags τ must be specified (see Section 7).

Following Stevenson et al. (2019), we use a buffer of $b = 2$ km, beyond which we assume no animal could enter the detection zone between the passage of the two observers. Stevenson et al. (2019) applied a Palm likelihood estimation approach, termed cluster capture-recapture (CCR). For comparison with their work we quote results for parameter σ_{palm} and mean animal speed: see Web Appendix C for the relationship between these parameters and the parameter σ used above. Stevenson et al. (2019) obtained the following estimates, with 95% confidence intervals in brackets: $\hat{D} = 1.05\ (0.84, 1.60)$ pods per km^2; $\hat{\sigma}_{palm} = 0.15\ (0.11, 0.19)$

km; and the expected proportion of time in the surface state, $\hat{\gamma} = 0.86$ $(0.56, 1.00)$. Using the LCE method, we obtain $\hat{D} = 1.24$ $(0.97, 1.60)$ pods per km^2, $\hat{\sigma}_{palm} = 0.09$ $(0.07, 0.11)$ km, and $\hat{\gamma} = 0.73$ $(0.55, 0.91)$. The estimate $\hat{\sigma}_{palm} = 0.09$ corresponds to a mean rate of displacement over $l = 248$ seconds of 0.58 m/s, with 95% confidence interval $(0.47, 0.71)$ m/s.

Stevenson et al. (2019) estimated the coefficients of variation (CV) of $\hat{D}$, $\hat{\sigma}_{palm}$ and $\hat{\gamma}$ to be 19%, 16%, and 13%, respectively. The corresponding estimated CVs from the LCE method are 13%, 10%, and 13%, respectively. The estimates from the two methods are broadly consistent; the LCE method estimates there to be substantially less animal movement, slightly less time at the surface, and a higher animal density. As we cannot evaluate the relative merits of the methods on the basis of a single survey with unknown density, we investigate their performance by simulation.

7. Simulation study

Recall that X_{i1} and X_{i2} are detections of animal i by two observers separated by a time lag. With lags close to zero, X_{i1} and X_{i2} are highly correlated because animals available to one observer are almost certain to be available to the other. As lag increases, we expect this correlation to decrease. A pertinent question is whether dependence can be removed by choosing a suitably long lag. To investigate this we look at the correlation between X_{i1} and X_{i2} as a function of lag, with γ values from 0.1 to 0.9, and lags from 0 to 500 seconds.

In our model, X_{i1} and X_{i2} are Bernoulli random variables with expectation $\gamma w/b$. The correlation between these variables when there is a separation of t seconds between the two observers passing over an animal, is

$$\rho(t) \;=\; \frac{\sum_{x_{i1}=0}^{1}\sum_{x_{i2}=0}^{1}\left(x_{i1}-\gamma\frac{w}{b}\right)\left(x_{i2}-\gamma\frac{w}{b}\right)\mathbb{P}(x_{i1},x_{i2}\mid t)}{\gamma\frac{w}{b}\left(1-\gamma\frac{w}{b}\right)}\,, \tag{14}$$

where $\mathbb{P}(x_{i1}, x_{i2} \mid t)$ is given in (8).

The dark line in Figure 2 shows the correlation as a function of the lag ($t = l$) for $\tau = 110$ seconds and γ and σ equal to the estimates obtained in the previous section. It also shows the correlation for $\gamma \in \{0.1, 0.2, \ldots, 0.9\}$ and the correlation under the assumption that animals do not move but do become unavailable by diving.

[Figure 2 about here.]

It is clear that increasing the lag to τ or more reduces correlation to approximately zero (grey lines) if animals do not move and we consider only animals within w of the transect line, although in the presence of animal movement (when we consider animals within b of the line) there is still correlation between observers due to in/out availability. The decay to zero corroborates the observation of Stevenson et al. (2019) that correlation between observers due to up/down availability can be removed by setting a lag greater than τ. With such long lags, the up/down availability model requires only the single parameter γ, corresponding to the proportion of time spent at the surface. This has the considerable advantage that there are no unidentifiable parameters, so no external data are needed to estimate density.

In practice, we are primarily interested in methods for surveys with two cameras on one aircraft, and with this configuration and fast-moving aircraft, lags of more than some tens of seconds are unlikely to be achievable. In light of this, and the results of Figure 2, we present simulations for (a) a scenario designed to imitate the porpoise survey above, and (b) scenarios with lag l of 10, 20, 50 and 80 seconds, and γ appoximately equal to, and bracketing, the estimates of γ obtained above, namely 0.5, 0.8, and 0.9. For σ we use values 15, 8 and 23, which correspond to the rounded mean of the estimated σ_{palm} from the LCE and CCR methods (in m), converted from σ_{palm} to σ (see Web Appendix C), and to rounded values that are 50% smaller and 50% larger, respectively. In all cases, we use the same τ in estimation as was used in simulation. For the short-lag scenarios in (b), we perform simulations with true density $D = 1.24$, as estimated in the previous section, and with an

observer speed of 100 knots, which is around the typical speed of marine aerial surveys such as the harbor porpoise survey above. We performed 1000 simulations for each scenario.

7.1 *Simulation based on harbor porpoise data: lag of 248 seconds*

For this scenario we use the estimates of Stevenson et al. (2019) as the generating values, corresponding to $D = 1.05$, $\gamma = 0.86$ and $\sigma_{palm} = 0.15$. Initial line length is $L = 1100$ km, which is subsequently doubled or tripled to increase sample sizes. We investigate by simulation the bias and precision of the LCE estimator. In the light of our results in Section 6, where we obtained an LCE estimate that was 18% greater than the CCR estimate of Stevenson et al. (2019), we also investigate whether this discrepancy is within the bounds expected due to estimator variability.

The empirical bias and CV of the LCE and CCR density estimators from 10^3 simulations are 9.9% (CV=29.8%) and 12.7% (CV=37.9%), respectively. The biases reduce to 4.3% (CV=18.0%) and 5.1% (CV=21.4%) when sample size is doubled while holding density constant, and to 2.9% (CV=14.6%) and 3.3% (CV=16.7%) when sample size is tripled.

The correlation between LCE and CCR density estimates from the simulations is 0.75, while the probability of getting a relative difference as large as, or larger than, that observed is approximately 20%, from which we conclude that the observed difference is not large enough to raise concerns about the validity of either estimator with the porpoise data.

The LCE estimator formulates the delay in encounter times between the two observers as a random variable, due to along-transect animal movement towards or away from the second observer, while the CCR method currently does not, and instead assumes these times to be equal to the lag time between the observers. We anticipate that this will cause the expected values of the two estimators to diverge for long lags, or for the case where animal speeds are non-negligible relative to observer speeds, and this may cause the CCR estimator of density to become biased. Here, however, with the observers moving some 50 times faster than the

animals, and the standard deviation of the difference between encounter lag and observer lag being only 2.4% of the observer lag, the effect on the CCR estimator is very small.

7.2 *Short lag scenarios*

Here we investigate the bias and confidence interval coverage of the LCE density estimator under short lag scenarios, and compare them with those obtained from the CCR estimator of Stevenson et al. (2019). There are 36 simulation scenarios corresponding to all combinations of lag $l \in \{10, 20, 50, 80\}$ seconds, $\gamma \in \{0.5, 0.8, 0.9\}$, and $\sigma \in \{8, 15, 23\}$. We set $L = 1100$ km, $w = 0.125$ km, and $\tau = 110$ s. Simulation results are summarized in Table 1. Boxplots of the LCE density estimates for each of the 36 scenarios are shown in Figure 3.

[Figure 3 about here.]

[Table 1 about here.]

The LCE density estimator is unbiased or nearly unbiased in all 36 scenarios. Figure 4 shows the empirical bias as a function of the mean number of detections by each observer, together with the empirical bias of the CCR estimator fitted to the same simulated data. The bias of the two estimators is very similar. The correlation between the two estimators varies from 0.576 to 0.871 across the 36 scenarios, and the mean difference of the estimator means from the true density, as a percentage of the true density, is 2.71% in the case of the LCE estimator, and 1.7% in the case of the CCR estimator.

[Figure 4 about here.]

The coefficients of variation of the LCE and CCR density estimators for all 36 scenarios are shown in Figure 5. The CVs decrease with sample size, as expected. The CV of the LCE estimator is less than that of the CCR estimator in all cases, the more so the larger the sample size. We interpret this to be a consequence of the fact that the CCR estimator is not a maximum likelihood estimator, being based instead on an approximation to the Palm

likelihood of pairwise comparisons between detections, so it does not have the asymptotic efficiency of a maximum likelihood estimator. Nevertheless, the difference in precision of the two estimators is very small.

[Figure 5 about here.]

In almost all cases coverage probability is close to 95% (Table 1), with coverage probability tending to be a bit worse when lag is short and there is greater movement (larger σ), and tending to be too high when animals are almost always available ($\gamma = 0.9$). We conclude that for these scenarios, the LCE estimator is approximately unbiased, with confidence interval coverage usually close to nominal, but slightly high when animals are almost always available. The performance of the LCE and CCR estimators is very similar, with the LCE estimator making a slight gain in precision as sample size increases.

8. Discussion

We have focused here on surveys for diving animals conducted by UAVs, but the LCE method is applicable to a broad range of survey scenarios. In its simplest formulation, our full model involves parameters D and σ for modeling density and animal movement, and three parameters for detection and availability: parameter p for detection of available animals, and parameters τ and γ to model availability via the diving cycle. Only one of the three parameters (p, τ, γ) is identifiable from the two-observer design (Stevenson et al., 2019), but in many survey scenarios this is not an impediment to application.

For our scenario, involving narrow-strip surveys of diving animals from UAVs, we set $p = 1$, obtained τ from external data, and estimated γ. For UAV surveys of non-diving animals, including land surveys, the parameters τ and γ are not needed, so parameter p can be estimated from the two-observer data. When animals on a terrestrial survey are missed because the view of them is obscured (by a bush, for example), the probability of being

obscured would be reflected in the estimate of p. This survey type is described as mark-recapture or double-count aerial surveys, and the new development offered by LCE is to accommodate animal movement and uncertain capture history into this design. For surveys with a wider field of view, for example from conventional aircraft, detection may decrease with distance from the trackline and the survey type is described as mark-recapture distance-sampling (MRDS). In this case, additional data are collected on the perpendicular distances of animals from the trackline, enabling additional parameters to be estimated which describe the decay of detections with distance. The LCE method provides a framework for MRDS surveys to incorporate animal movement and uncertain capture histories, developments that have been recommended in previous work (Burt et al., 2014).

The LCE method has some advantages over the CCR method, but its computation time does not scale well as density increases. While we were able to deal with moderately large sample sizes above, this is because density was low enough that the transect line could be divided into many segments with relatively few possible combinations of capture histories within each segment. The number of possible capture histories increases very rapidly when each observer detects more than a few animals within a segment, and computation by the LCE method will be infeasible in this case. The number of possible capture histories is $N_{CH} = \sum_{m=0}^{n_2^*} \binom{n_2^*}{m} n_1^*!/(n_1^* - m)!$, where n_1^* is the larger of n_1 and n_2, and n_2^* is the smaller. As n_1^* increases, the LCE estimation method will become too slow to be practically useful on typical desktop computers. The CCR method, by contrast, scales well and is able to deal with much larger numbers of detections.

Being a maximum likelihood method, the LCE method has the advantage of being able to use the extensive inference results and machinery associated with maximum likelihood, including asymptotic efficiency and likelihood-based variance estimators and model-selection criteria such as AIC. The CCR estimator is slightly less efficient than the LCE estimator

for large sample sizes, requires variance estimation by bootstrap, and cannot take advantage of likelihood-based model selection tools. It does not currently accommodate varying times between encounters of animals due to animal movement, although in the scenarios we considered this has negligible effect – this will be important for much slower-moving observers. Finally, the LCE method provides an inference framework that allows inclusion of covariates in all parameters mentioned in Section 4.1. While covariates were not available for our application, we anticipate that they may be collected on future surveys.

The major advantage of both the LCE and the CCR frameworks is that they do not require duplicate sightings to be identified between the two observers. We anticipate that this will facilitate substantial reduction in the cost of processing double-observer data, because it allows the estimation process to be automated. For automatic processing we only need an adequate automatic identifier of the target species in each of the two separate video streams. Since false positives are not handled by our framework, criteria for automated object identification must be set conservatively so that the false-positive rate is reduced almost to zero. This will have the effect of lowering the detection probability, p, so we will not be able to assume that $p = 1$. As described above, p is estimable from the data if there is no dive-cycle model, and potentially estimable even in the presence of a dive-cycle model if a varying-lag design is employed. It is therefore likely that fully-automated survey processing will become achievable in the near future, commensurate with advances in object identification algorithms and UAV engineering.

Additional supporting information may be found online in the Supporting Information section at the end of the article.

Acknowledgements

This work was part-funded by the Royal Society of New Zealand Marsden grant UOA-1418, Leverhulme grant `RF-2018-213\9` and EPSRC IAA grant 'High Definition digital aerial

survey software'. Stephen Marsland contributed to the derivation of $f_T(t)$.

Data Availability

Data sharing is not applicable to this article as no new data were created or analyzed in this paper.

References

Bonner, S. J. and Holmberg, J. (2013). Mark-recapture with multiple, non-invasive marks. *Biometrics* **69,** 766–75.

Borchers, D. L. and Langrock, R. (2015). Double-observer line transect surveys with Markov-modulated Poisson process models for overdispersed animal availability. *Biometrics* **71,** 1060–1069.

Borchers, D. L., Zucchini, W., Heide-Jørgenssen, M. P., Canadas, A., and Langrock, R. (2013). Using hidden Markov models to deal with availability bias on line transect surveys. *Biometrics* **69,** 703–713.

Burt, M. L., Borchers, D. L., Jenkins, K., and Marques, T. A. (2014). Using mark-recapture distance sampling methods on line transect surveys. *Methods in Ecology and Evolution* **5,** 1180–1191.

Fewster, R. M., Stevenson, B. C., and Borchers, D. L. (2016). Trace-contrast models for capture-recapture without capture histories. *Statistical Science* **31,** 245–258.

Hamilton, O. N. P., Kincaid, S. E., Constantine, R., Kozmian-Ledward, L., Walker, C. G., and Fewster, R. M. (2018). Accounting for uncertainty in duplicate identification and group size judgements in mark-recapture distance sampling. *Methods in Ecology and Evolution* **9,** 354–362.

Hammond, P. S., Lacey, C., Gilles, A., Viquerat, S., Börjesson, P., Herr, H., Macleod, K., Ridoux, V., Santos, M. B., Scheidat, M., Teilmann, J., Vingada, J., and Øien, N. (2017).

Estimates of cetacean abundance in European Atlantic waters in summer 2016 from the SCANS-III aerial and shipboard surveys. Technical report, University of St Andrews.

Henkel, L. A., Ford, R. G., Tyler, W. B., and David, J. N. (2007). Comparison of aerial and boat-based survey methods for marbled murrelets *Brachyramphus marmoratus* and other marine birds. *Journal of Marine Ornithology* **35,** 145–151.

Hiby, L. and Lovell, P. (1998). Using aircraft in tandem formation to estimate abundance of harbour porpoise. *Biometrics* **54,** 1280–1289.

Langrock, R., Borchers, D. L., and Skaug, H. (2013). Markov-modulated nonhomogeneous Poisson processes for unbiased estimation of marine mammal abundance. *Journal of the American Statistical Association* **108,** 840–851.

Link, W., Yoshizaki, J., Bailey, L., and Pollock, K. (2010). Uncovering a latent multinomial: analysis of mark-recapture data with misidentification. *Biometrics* **66,** 178–185.

Pike, D. and Doniol-Valcroze, T. (2015). Identification of duplicate sightings from the 2013 double-platform High Arctic Cetacean Survey. Technical report, DFO Canadian Science Advisory Secretariat. Doc 2015/034.

Stevenson, B. C., Borchers, D. L., and Fewster, R. M. (2019). Cluster capture-recapture to account for identification uncertainty on aerial surveys of animal populations. *Biometrics* **75,** 326–336.

Tanaka, U., Ogata, Y., and Stoyan, D. (2008). Parameter estimation and model selection for Neyman-Scott point processes. *Biometrical Journal* **50,** 43–57.

Zhang, W., Bravington, M. V., and Fewster, R. M. (2019). Fast likelihood-based inference for latent count models using the saddlepoint approximation. *Biometrics* **75,** 723–733.

Zucchini, W., MacDonald, I. L., and Langrock, R. (2016). *Hidden Markov Models for Time Series: An Introduction Using R, Second Edition.* Chapman and Hall/CRC.

Supporting Information

Web Appendices A-C referenced in Sections 2, 5, 6 and 7 above are available with this paper at the Biometrics website on Wiley Online Library. Appendix A contains the derivation of $f_T(t)$, Appendix B describes the constraint programming method for enumerating all $\boldsymbol{\omega}^{(m)}$, and Appendix C derives the relationship between σ_{palm}, σ and mean animal speed. Appendix D describes the availability of code on GitHub that reproduces the results of this paper.

The code and data used for the analyses in this paper are available at the Biometrics website on Wiley Online Library.

Received ?? 2019. *Revised* 20??

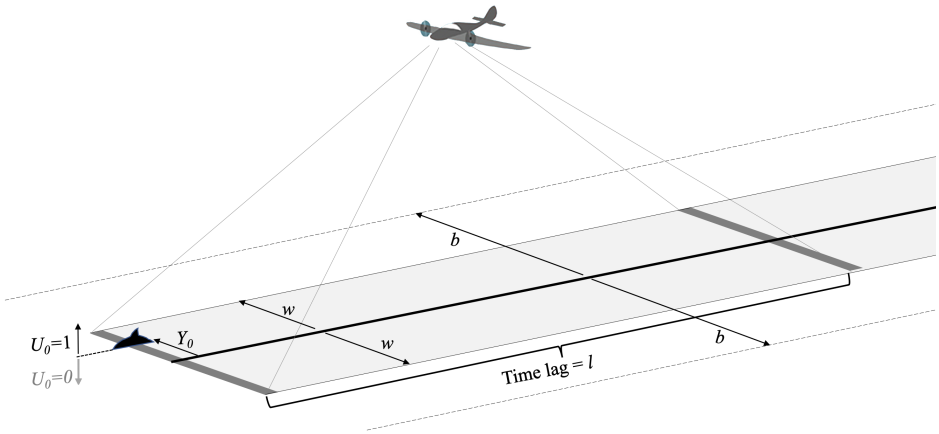

Figure 1. Illustration of the two-camera survey design, here with both cameras mounted on a single aircraft. Both cameras cover the grey strip, separated by a time lag l. This detection zone has half-width w. The fields of view of the cameras are indicated by dark grey strips spanning the width of the detection zone. It may be possible for animals within a wider strip of half-width b to move into or out of the grey strip between the passing of the first and second camera. Y_0 is the distance to the right of the trackline (the dark black centre line), of an animal at the time it comes into the first camera's field of view ($t = 0$) and U_0 is its surface state at this time: $U_0 = 1$ if the animal is in the near-surface state and $U_0 = 0$ if not. The animal's distance and surface state at times $t > 0$ are Y_t and U_t, respectively. The random variable Z_t is defined to be 1 if the animal is in the detection zone at time t ($|Y_t| \leqslant w$), and 0 otherwise.

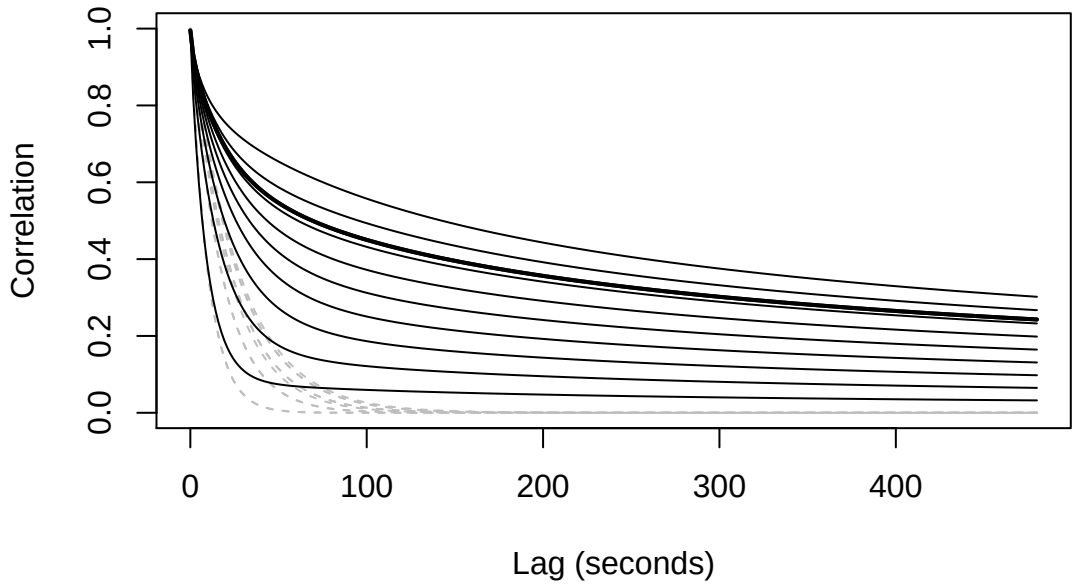

Figure 2. Correlation between detections by the two observers as a function of lag for mean proportions of time available $\gamma = 10\%$ (bottom black line), $20\%, 30\%, 40\%, 50\%, 60\%, 70\%, 80\%, 90\%$ (top black line). The thick black line is for $\gamma = 73\%$. The grey dashed lines show the correlation under the assumption of no animal movement, for which there is no in/out process and $b = w$.

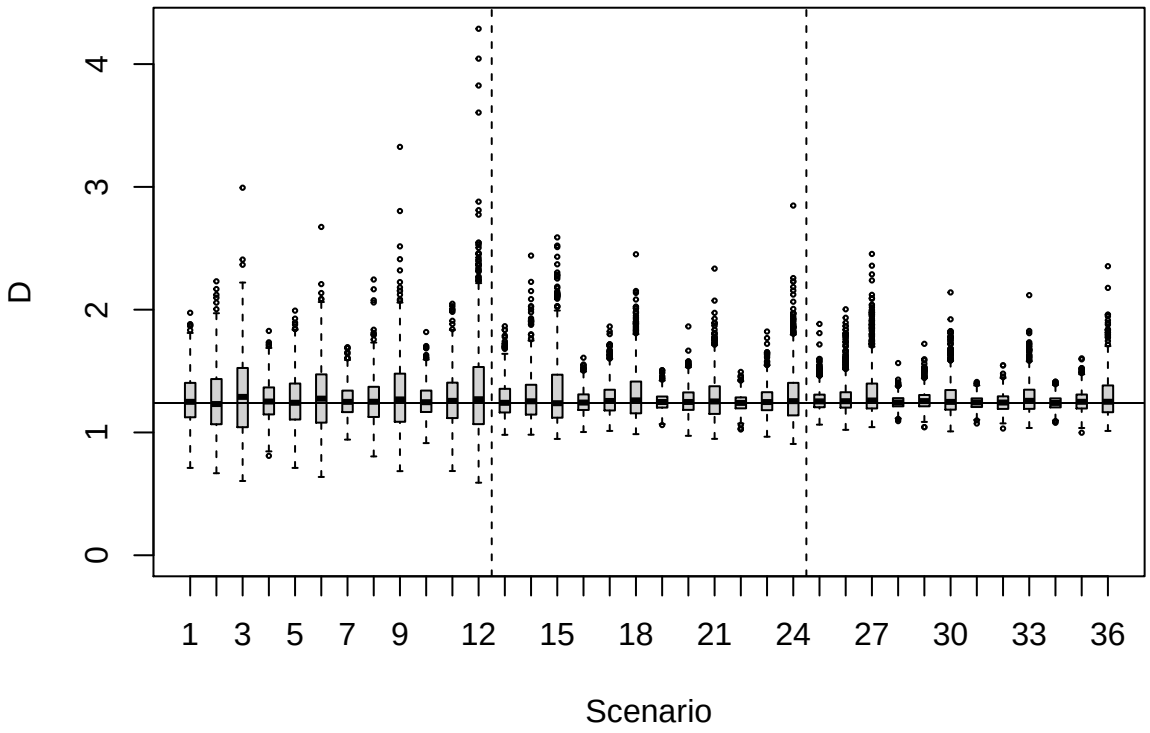

Figure 3. Box plots of estimated LCE density for each of the 36 scenarios. The horizontal line is at true density $D = 1.24$. Scenarios are numbered in the same order as they appear in Table 1. Vertical dashed lines separate simulations according to the three sample size groups shown in Figures 4 and 5.

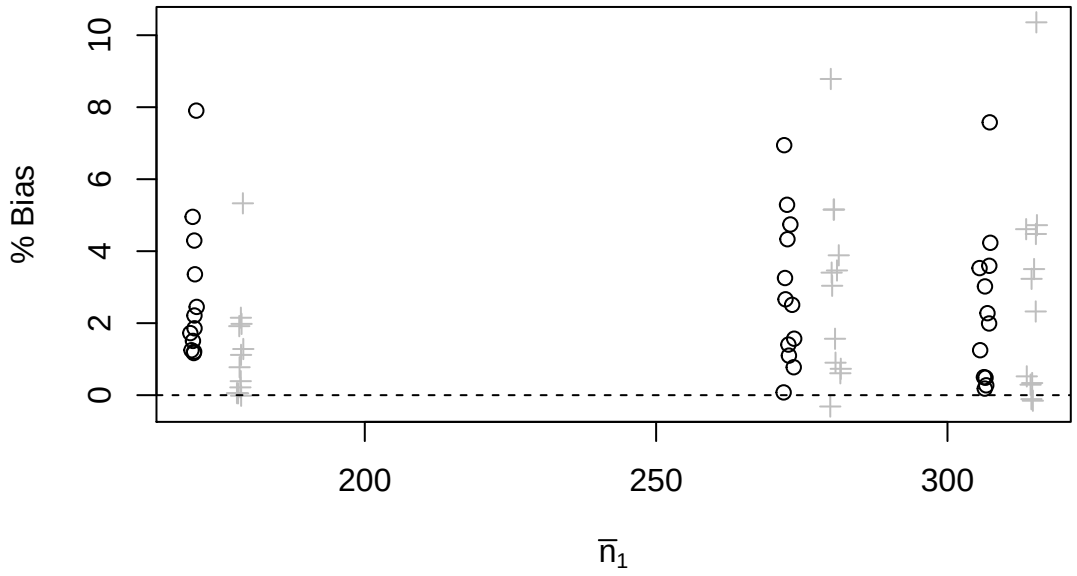

Figure 4. Percentage difference of estimated density from true density, as a function of mean number of detections by a single observer. The LCE estimator is represented by circles, the CCR estimator by crosses. Crosses are offset 8 points to the right, to avoid overlap with circles. From left to right, the mean percentage difference within each of the three groups of estimates is 2.8, 2.9 and 2.4 in the case of the LCE estimator, and 1.3, 3.0 and 2.8 in the case of the CCR estimator

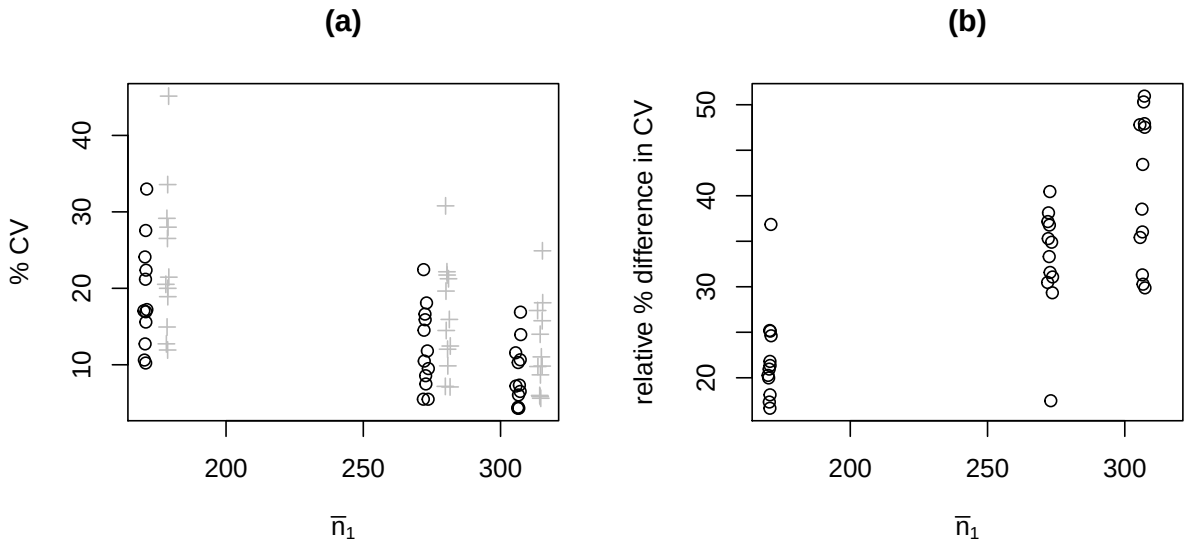

Figure 5. Percentage coefficient of variation (%CV), as a function of mean number of detections by a single observer. The LCE estimator is represented by circles, the CCR estimator by crosses. Crosses are offset 8 units to the right, to avoid overlap with circles. Panel (a) shows the %CV. Panel (b) shows the amount by which the CV from the CCR method exceeds that from the LCE method, expressed as a percentage of the LCE CV.

Table 1

Simulation results for LCE and CCR estimators from 1,000 simulations. Here gamma is the proportion of time animals are available, dive cycle length is 110 seconds, lag is the time between observers, sigma is the animal diffusion rate parameter, mean(n) and mean(m) are the mean numbers of detections by one observer and the mean number of recaptures, across simulations.

	gamma	lag	sigma	%BiasLCE	%cvLCE	%CoverLCE	%BiasCCR	%cvCCR	mean(n)	mean(m)
1	0.50	10.00	8.00	2.21	16.93	0.95	1.12	20.00	170.77	132.86
2	0.50	10.00	15.00	1.17	21.19	0.93	0.22	26.52	170.65	122.80
3	0.50	10.00	23.00	4.30	27.56	0.90	2.15	33.57	170.74	111.29
4	0.50	20.00	8.00	1.51	12.73	0.95	0.78	14.94	170.51	111.97
5	0.50	20.00	15.00	1.72	17.07	0.94	0.06	20.53	170.06	99.12
6	0.50	20.00	23.00	3.36	22.38	0.93	1.98	28.00	170.85	85.25
7	0.50	50.00	8.00	1.21	10.23	0.96	0.39	11.93	170.72	81.12
8	0.50	50.00	15.00	1.86	15.58	0.96	-0.02	18.91	170.78	66.02
9	0.50	50.00	23.00	4.95	24.10	0.94	1.92	29.16	170.46	51.06
10	0.50	80.00	8.00	1.25	10.62	0.95	0.05	12.74	170.26	69.23
11	0.50	80.00	15.00	2.45	17.22	0.95	1.28	21.46	171.15	52.54
12	0.50	80.00	23.00	7.90	32.99	0.92	5.33	45.14	171.08	39.22
13	0.80	10.00	8.00	2.51	11.81	0.95	3.89	15.93	273.34	229.51
14	0.80	10.00	15.00	4.33	15.89	0.91	5.16	21.74	272.54	211.30
15	0.80	10.00	23.00	6.94	22.44	0.86	8.78	30.79	271.98	190.81
16	0.80	20.00	8.00	1.10	7.49	0.98	0.90	9.86	272.79	209.18
17	0.80	20.00	15.00	2.66	10.49	0.95	3.04	14.48	272.21	185.03
18	0.80	20.00	23.00	5.29	16.63	0.93	5.15	22.17	272.47	158.80
19	0.80	50.00	8.00	0.78	5.49	0.98	0.61	7.10	273.61	181.84
20	0.80	50.00	15.00	1.41	8.57	0.96	1.57	12.04	272.70	146.84
21	0.80	50.00	23.00	3.25	14.52	0.95	3.40	19.64	272.12	114.33
22	0.80	80.00	8.00	0.08	5.50	0.98	-0.32	7.17	271.88	168.45
23	0.80	80.00	15.00	1.57	9.50	0.96	0.73	12.45	273.69	128.56
24	0.80	80.00	23.00	4.74	18.09	0.92	3.46	21.25	273.04	94.71
25	0.90	10.00	8.00	2.28	7.34	0.99	3.50	11.03	306.86	264.08
26	0.90	10.00	15.00	3.59	10.65	0.98	4.48	15.76	307.17	244.15
27	0.90	10.00	23.00	7.58	16.88	0.95	10.36	24.91	307.25	221.46
28	0.90	20.00	8.00	0.50	4.32	0.99	0.29	5.99	306.26	247.58
29	0.90	20.00	15.00	1.99	6.51	0.98	2.32	9.83	307.15	220.34
30	0.90	20.00	23.00	3.53	11.57	0.96	4.61	17.10	305.50	188.14
31	0.90	50.00	8.00	0.27	4.31	0.99	-0.15	5.62	306.65	226.09
32	0.90	50.00	15.00	0.48	6.05	0.99	0.34	8.68	306.53	183.73
33	0.90	50.00	23.00	3.02	10.29	0.95	3.23	14.00	306.43	142.15
34	0.90	80.00	8.00	0.18	4.45	0.99	-0.11	5.85	306.40	212.91
35	0.90	80.00	15.00	1.25	7.22	0.97	0.52	9.77	305.61	160.81
36	0.90	80.00	23.00	4.23	13.94	0.90	4.72	18.11	307.35	119.72